Phase field approach to interaction of phase transformation and dislocation evolution

Valery I. Levitas and Mahdi Javanbakht

Citation: Appl. Phys. Lett. **102**, 251904 (2013); doi: 10.1063/1.4812488
View online: http://dx.doi.org/10.1063/1.4812488
View Table of Contents: http://apl.aip.org/resource/1/APPLAB/v102/i25
Published by the AIP Publishing LLC.

Phase field approach to interaction of phase transformation and dislocation evolution

Valery I. Levitas[1] and Mahdi Javanbakht[2]
[1]*Departments of Aerospace Engineering, Mechanical Engineering, and Material Science and Engineering, Iowa State University, Ames, Iowa 50011, USA*
[2]*Department of Mechanical Engineering, Iowa State University, Ames, Iowa 50011, USA*

(Received 23 May 2013; accepted 12 June 2013; published online 25 June 2013)

Phase field approach to coupled evolution of martensitic phase transformations (PTs) and dislocation is developed. A fully geometrically nonlinear formulation is utilized. The finite element method procedure is developed and applied to study the hysteretic behavior and propagation of an austenite (A)–martensite (M) interface with incoherency dislocations, the growth and arrest of martensitic plate for temperature-induced PT, and the evolution of phase and dislocation structures for stress-induced PT. A similar approach can be developed for the interaction of dislocations with twins and diffusive PTs described by Cahn-Hilliard theory. © *2013 AIP Publishing LLC*. [http://dx.doi.org/10.1063/1.4812488]

Various material phenomena related to interaction between martensitic phase transformations (PTs) and dislocational plastic deformation are of fundamental and technological importance. Examples are: heat and thermomechanical treatment of material to obtain desired structure and properties; transformation-induced plasticity;[1] synthesis of materials under high pressure and high pressure with large plastic deformations, e.g., during ball milling[2] and in rotational diamond anvil cell;[3,4] and PTs during friction, indentation, surface treatment, and projectile penetration. With the development of nanoscience and technology, PT and plasticity are studied in nanoparticles, films, wires, and for smart nanosystems. The interaction between PT and dislocations drastically changes PT thermodynamics, kinetics, and microstructure and is the most basic problem in the study of M nucleation and growth kinetics, PT hysteresis, and irreversibility, i.e., region of metastability of phases.[4,5] In particular, M nucleation occurs at various dislocation configurations. An A–M interface loses its coherency through the nucleation of dislocations. Interaction between PT and plasticity is also a key point in developing materials with high strength and ductility,[6] in particular, utilizing transformation toughening.

Phase field approach (PFA) is broadly used for simulations of PTs[7–9] and dislocation evolution.[10,11] There are a few simplified PFA approaches to study the interaction between PT and dislocations. There are a number of analytical treatments of M nucleation on dislocations based on PFA to PT,[12] followed by numerical[13] simulations. Dislocations are introduced through their stationary stress field or are located at the moving phase interface only[14] and therefore do not require additional PFA equations. In Ref. 11, we solved some problems on interactions between PT and evolving dislocations using a simplified version of PFA. Thus, there currently is no PFA to interaction between PT and evolving dislocations.

Here, a coupled PFA to martensitic PT and dislocation evolution is developed as a combination of the most advanced PFA for PT[9] and dislocations[11] with nontrivial coupling terms. It is based on large strain formulation and utilizes other advantages of Refs. 9 and 11: advanced thermodynamic potential that describes some conceptual features of the effect of the stress tensor, reproducing, in particular, the stress-independent transformation strain tensor and Burgers vector and desired local stress-strain curve. Also, the desired, mesh-independent, dislocation height is introduced for any slip orientation, leading to a well-posed formulation. Coupling between PT and dislocations includes nonlinear kinematics and corresponding mechanical driving forces, *inheritance* of dislocation during PT, and the dependence of all material parameters for dislocations on the order parameter η that describes PT, which results also in the extra driving force for PT due to the change in dislocation energy during the PT. Finite element method (FEM) procedure is developed and applied to the following problems: (a) Hysteretic behavior and propagation of an A–M interface with evolving incoherency dislocations for *temperature-induced* PT (i.e., without external stresses). *Scale-dependent athermal hysteresis* is determined, and the *mechanism* of the interface motion through dislocation obstacles is revealed. These results can be utilized for controlling the region of metastability of phases. (b) Evolution of phase and dislocation structures for *stress-induced* PT. Dislocations are *pushed* by the moving interface for small angles between the slip direction and the interface normal and penetrate through the interface and are *inherited* by the product phase for large angles. (c) M plate growth with the generation of dislocations at its tip. At higher temperature, dislocations arrest the plate, exhibiting athermal friction. When this friction can be overcome at lower temperature, the width of the M plate is larger than in the case without dislocations due to stress relaxation.

We designate contractions of tensors $\boldsymbol{A}$ and $\boldsymbol{B}$ over one and two indices as $\boldsymbol{A}\cdot\boldsymbol{B}$ and $\boldsymbol{A}:\boldsymbol{B}$; the transpose of $\boldsymbol{A}$ is $\boldsymbol{A}^T$, $\boldsymbol{I}$ is the unit tensor, and $\otimes$ is a dyadic product.

Model. Let the motion of an elastoplastic material with PT be described by equation $\boldsymbol{r}=\boldsymbol{r}(\boldsymbol{r}_0,t)$, where $\boldsymbol{r}$ and $\boldsymbol{r}_0$ are the positions of a material point at time t (deformed configuration V) and t_0 (undeformed configuration V_0, which is in A state). All equations are considered in V_0. Multiplicative decomposition of the deformation gradient into elastic,

transformational, and plastic parts is used: $\boldsymbol{F} = \partial \boldsymbol{r}/\partial \boldsymbol{r}_0 = \boldsymbol{F}_e \cdot \boldsymbol{F}_t \cdot \boldsymbol{F}_p$. Transformation $\boldsymbol{F}_t$ and plastic $\boldsymbol{F}_p$ deformation gradients are described as[9,11]

$$\mathbf{F}_t = \mathbf{I} + \boldsymbol{\varepsilon}_t(a\eta^2(1-\eta)^2 + (4\eta^3 - 3\eta^4)), \tag{1}$$

$$\dot{\boldsymbol{F}}_p \cdot \boldsymbol{F}_p^{-1} = \sum_{\alpha=1}^{p}\sum_{\omega=1}^{m_\alpha} \frac{1}{H^\alpha} \boldsymbol{b}^{\alpha\omega} \otimes \boldsymbol{n}^\alpha \dot{\phi}(\bar{\xi}_{\alpha\omega}). \tag{2}$$

The order parameter η for PT varies from 0 (in A) to 1 (in M); the order parameter $\xi_{\alpha\omega}$ for dislocations in the αth plane with the unit normal $\boldsymbol{n}^\alpha$ along the ωth slip direction with the Burgers vector $\boldsymbol{b}^{\alpha\omega}$ varies from 0 to n when n dislocations appear; $Int(\xi_{\alpha\omega}) = n$ and $\bar{\xi}_{\alpha\omega} := \xi_{\alpha\omega} - Int(\xi_{\alpha\omega}) \in [0,1]$ are the integer and fractional parts of $\xi_{\alpha\omega}$. In Eqs. (1) and (2), $\varepsilon_t = \boldsymbol{F}_t(1) - \boldsymbol{I}$ is the transformation strain, a is the parameter, $\phi(\bar{\xi}) = \bar{\xi}^2(3-2\bar{\xi})$, and H^α is the dislocation height. For compactness, we consider a single M variant only; generalization for multiple M variants can be done as in Ref. 9. The Helmholtz free energy per unit undeformed volume is accepted as the sum of elastic, thermal, crystalline, and gradient energies related to PT and dislocations

$$\psi = \psi^e + f + \psi_\eta^\nabla + \psi_\xi + \psi_\xi^\nabla, \tag{3}$$

$$\psi_\xi = \sum_{\alpha=1}^{p}\sum_{\omega=1}^{m_\alpha} A_\alpha(\eta)\bar{\xi}_{\alpha\omega}^2(1-\bar{\xi}_{\alpha\omega})^2, \tag{4}$$

$$\psi_\eta^\nabla = 0.5\beta_\eta|\nabla\eta|^2; \quad \psi_\xi^\nabla = 0.5\beta_\xi(\eta) \times \sum_{\alpha=1}^{p}\sum_{\omega=1}^{m_\alpha}\{\nabla\bar{\xi}_{\alpha\omega}^2 + [M(1-\bar{\xi}_{\alpha\omega})^2 - 1](\nabla\bar{\xi}_{\alpha\omega}\cdot\boldsymbol{n}_\alpha)^2\}, \tag{5}$$

$$f = A_0(\theta-\theta_e)\phi(\eta)/3 + A_0(\theta_e-\theta_c)\eta^2(1-\eta)^2. \tag{6}$$

Here, θ, θ_e, and θ_c are the temperature, the A-M equilibrium temperature, and the critical temperature for the loss of A stability, respectively; β_ξ and β_η are the gradient energy coefficients; and A_0 and M are the parameters. The coefficient A_α, which determines the nucleation barrier for dislocations, is a periodic step-wise function of the coordinate along $\boldsymbol{n}_\alpha$.[11] The thermodynamic procedure similar to that in Refs. 8, 9, and 11 results in the elasticity rule for the nonsymmetric Piola-Kirchhoff stress tensor (force per unit area in V_0) $\boldsymbol{P} \cdot \boldsymbol{F}_p^T \cdot \boldsymbol{F}_t^T = \frac{\partial\psi}{\partial \boldsymbol{F}_e}$ and expressions for the dissipation rate due to PTs $D_\eta = X_\eta\dot{\eta} \geq 0$ and dislocations $D_\xi = X_{\alpha\omega}\dot{\xi}_{\alpha\omega} \geq 0$. Then, the simplest linear relationships between thermodynamic forces and rates lead to the Ginzburg-Landau equations

$$\frac{1}{L_\eta}\frac{\partial\eta}{\partial t} = X_\eta = \boldsymbol{P}^T \cdot \boldsymbol{F}_e : \frac{\partial \boldsymbol{F}_t}{\partial\eta}\cdot\boldsymbol{F}_p + \nabla\cdot\left(\frac{\partial\psi}{\partial\nabla\eta_i}\right) - \frac{\partial\psi}{\partial\eta}, \tag{7}$$

$$\frac{1}{L_\xi(\eta)}\frac{\partial\xi_{\alpha\omega}}{\partial t} = X_{\alpha\omega} = \boldsymbol{P}^T\cdot\boldsymbol{F}_e : \boldsymbol{F}_t\cdot\frac{\partial\boldsymbol{F}_p}{\partial\xi_{\alpha\omega}} + \nabla\cdot\left(\frac{\partial\psi}{\partial\nabla\xi_{\alpha\omega}}\right) - \frac{\partial\psi}{\partial\xi_{\alpha\omega}}, \tag{8}$$

where L_ξ and L_η are the kinetic coefficients. All parameters in the equations for dislocations depend on η according to the rule $B = B_A + (B_M - B_A)\phi(\eta)$, where B_A and B_M are the values of a parameter in A and M. This leads to contributions of the dislocation-related terms in Ginzburg-Landau Eq. (7) for PT. In addition, both processes are coupled through the mechanical driving force (stress power) in Eqs. (7) and (8) and the evolving stress field.

Slip systems of A ($\boldsymbol{b}_A^{\alpha\omega}$, $\boldsymbol{n}_A^{\alpha\omega}$) and M ($\boldsymbol{b}_M^{\alpha\omega}$, $\boldsymbol{n}_M^{\alpha\omega}$) are different and one needs to include both of them at each point (see Fig. S1 in Ref. 16 for details). Since all equations are defined in V_0, one has to pull back $\boldsymbol{b}_M^{\alpha\omega}$ and $\boldsymbol{n}_M^{\alpha\omega}$ into the undeformed A state: $\boldsymbol{b}_{MA}^{\alpha\omega} = \boldsymbol{F}_t^{-1}\cdot\boldsymbol{b}_M^{\alpha\omega}$ and $\boldsymbol{n}_{MA}^{\alpha\omega} = \boldsymbol{n}_M^{\alpha\omega}\cdot\boldsymbol{F}_t/|\boldsymbol{n}_M^{\alpha\omega}\cdot\boldsymbol{F}_t|$. When a diffuse A–M interface passes through dislocations in A, they are inherited by M and their Burgers vector, and normal to slip plane transforms into $\boldsymbol{b}_{AM}^{\alpha\omega} = \boldsymbol{F}_t\cdot\boldsymbol{b}_A^{\alpha\omega}$ and $\boldsymbol{n}_{AM}^{\alpha\omega} = \boldsymbol{n}_A^{\alpha\omega}\cdot\boldsymbol{F}_t^{-1}/|\boldsymbol{n}_M^{\alpha\omega}\cdot\boldsymbol{F}_t^{-1}|$. However, since all equations are referred to V_0, pulling $\boldsymbol{b}_{AM}^{\alpha\omega}$ and $\boldsymbol{n}_{AM}^{\alpha\omega}$ back into V_0 transforms them back into ($\boldsymbol{b}_A^{\alpha\omega}$, $\boldsymbol{n}_A^{\alpha\omega}$), i.e., no transformation is necessary. When a diffuse interface passes through dislocations in M, they are inherited by A and ($\boldsymbol{b}_M^{\alpha\omega}$, $\boldsymbol{n}_M^{\alpha\omega}$) transform into ($\boldsymbol{b}_{MA}^{\alpha\omega}$, $\boldsymbol{n}_{MA}^{\alpha\omega}$), which one already has, i.e., no transformation is needed. Thus, one has to define at each material point slip systems of A ($\boldsymbol{b}_A^{\alpha\omega}$, $\boldsymbol{n}_A^{\alpha\omega}$), and after pulling back into V_0, slip systems of M ($\boldsymbol{b}_{MA}^{\alpha\omega}$, $\boldsymbol{n}_{MA}^{\alpha\omega}$) (see Fig. S1(c) in Ref. 16), neither of which (as well as dislocation height H_α) depends on η. If inherited dislocations do not belong to the favorable slip system of the given phase, their yield strength is much higher or their motion may be arrested completely ($L_\xi = 0$). In the particular case when slip systems ($\boldsymbol{b}_A^{\alpha\omega}$, $\boldsymbol{n}_A^{\alpha\omega}$) and ($\boldsymbol{b}_{AM}^{\alpha\omega}$, $\boldsymbol{n}_{AM}^{\alpha\omega}$) coincide (i.e., they transform together with the crystal lattice during the PT), only one of them should be taken into account (see Fig. S2 in Ref. 16). This case will be considered in examples.

The equilibrium equation $\nabla\cdot\boldsymbol{P} = 0$ completes our system. Cubic-tetragonal PT was considered. Isotropic quadratic elastic potential ψ^e in terms of Lagrangian elastic strain $\boldsymbol{E_e} = (\boldsymbol{F}_e^T\cdot\boldsymbol{F}_e - \boldsymbol{I})/2$ with shear modulus $\mu = 71.5\,\text{GPa}$ and bulk modulus $K = 112.6\,\text{GPa}$ (the same for both phases) was used for below. The following parameters for PT and all slip systems have been used in all problems:[9,11] $L_\xi = 10^4(\text{Pa}\cdot\text{s})^{-1}$, $M = 0.1$, $H = 0.7\,\text{nm}$, $|\boldsymbol{b}| = 0.35\,\text{nm}$, $\beta_\eta = 2.59\times10^{-10}\,\text{N}$, $L_\eta = 2600\,(\text{Pa}\cdot\text{s})^{-1}$, $a = 3$, $\theta_e = 215\,\text{K}$, and $\theta_c = -183\,\text{K}$.

Numerical solutions. FEM approach and the code COMSOL with the embedded remeshing procedure have been utilized. Plane strain problems and straight edge dislocations are considered below. All size and time parameters are normalized by 1nm and 1ps, respectively. Boundary conditions are $\nabla\eta\cdot\boldsymbol{k} = \nabla\xi\cdot\boldsymbol{k} = 0$, where $\boldsymbol{k}$ is the normal to an external boundary in V_0. The upper side of a rectangle is fixed in the y direction and the lower side in both directions; lateral sides are stress-free; in problems (a) and (c3, shear stress is zero at the upper side. All results are shown in the deformed configuration.

Propagation of a semicoherent A–M interface: A rectangle with the size of 8×24 is considered. First, a stationary solution for the horizontal diffuse A–M interface was obtained in the middle of the sample without dislocations (Fig. 1). Transformation (misfit) strain of $\delta = 0.1$ in the x direction is applied only. We use $\beta_\xi = 8.76\times10^{-11}\,\text{N}$, $A_\alpha = 1.43\,\text{GPa}$ for A, $A_\alpha = 4.29\,\text{GPa}$ for M, and $\gamma = |\boldsymbol{b}|/H = 0.5$.

A dislocation band with the initial condition $\xi = 0.01$ is located at the initial phase interface. Incoherency dislocations

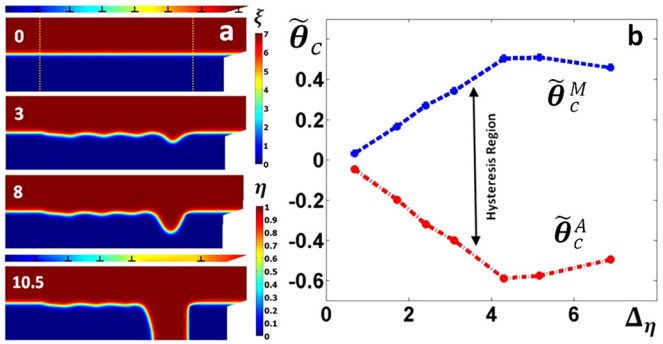

FIG. 1. (a) Coupled evolution of the PT order parameter η and dislocations for a semicoherent A–M interface at time instants shown in the corner. Thin band above the sample shows evolution of dislocations in the slip band along the initial A–M interface. (b) Dependence of the critical dimensionless temperature $\tilde{\theta}_c$ (athermal friction) causing interface motion until complete PT on the interface width Δ_η.

nucleate at the free surface and propagate along the interface. In the stationary state (Fig. 1), spacing between dislocations is 3.5, in perfect correspondence with $|\boldsymbol{b}|/\delta$. Both stationary solutions for the A–M interface and dislocations are taken as initial conditions for a coupled problem. To avoid the effect of the free surface on the A–M interface, we excluded PT from the two regions of the size of 8×4 at both ends of the sample (Fig. 1). Evolution of the PT for $\Delta_\eta = 9.17$ $\sqrt{\beta_\eta/(A_0(\theta_e - \theta_c))} = 1.7$ and the dimensionless temperature $\tilde{\theta} = (\theta_e - \theta)/(\theta_e - \theta_c) = 0.18$ for semicoherent A–M interface is shown in Fig. 1(a). Dependence of the critical temperature $\tilde{\theta}_c$ to cause interface motion until complete PT in a sample vs. Δ_η is presented in Fig. 1(b). Without dislocations, the coherent A–M interface is stable only at the specific temperature $\tilde{\theta}_c \simeq 0$, which is almost independent of Δ_η. A semicoherent A–M interface does not move in the range $\tilde{\theta}_c^A < \tilde{\theta} < \tilde{\theta}_c^M$, exhibiting an athermal friction. Interface starts motion (at $\tilde{\theta} > \tilde{\theta}_c^M$ toward A and at $\tilde{\theta} < \tilde{\theta}_c^A$ toward M) by penetration between two dislocations that increase spacing between them. After an interface reaches a horizontal sample's surface, it spreads laterally. In some cases, such a penetration occurs in two places simultaneously. Thus, an incoherent interface transforms to a coherent one and leaves dislocations behind. Surprising size dependence of an athermal friction, with maximum at $\Delta_\eta = 4.2$ is revealed. The unexpected point is that the macroscopic parameter $\tilde{\theta}_c$ strongly depends on the ratio Δ_η of two nanometer size parameters, which are usually considered to be zero. These results can be utilized for controlling the region of metastability of phases and can be transferred into a larger scale sharp incoherent interface model.[17]

Interaction of A–M interface with evolving dislocations for stress-induced PT: We consider a rectangular sample of the size of 36×15 that contains a rectangular region of the size of 30×5.6 at the center in which all equations are solved and outside of which dislocations are not included; also, outside of the region of the size of 30×9 at the center, PT is not included either, and only the elastic problem is solved. A parallel horizontal dislocation system is considered with initial $\xi = 0.01$. A horizontal displacement $u = 1.4 + t$ is applied at the upper side from $t = 0$ to 1.4 and then $u = 2.8$ from $t = 1.4$ to 1.7. Material parameters are: $\beta_\xi = 1.09 \times 10^{-10}$ N, $A_\alpha = 0.894$ GPa, $\gamma = 0.25$, $A_0 = 4.4$ MPa K^{-1}, $\varepsilon_t^y = 0.1$, $\varepsilon_t^x = -0.05$. For PT in shape memory alloys, M has significantly lower yield strength than A; we will study the limit case when dislocation evolution is completely arrested in A by using $L_\xi = L\,\eta$. The initial condition for PT corresponds to the sharp vertical A–M interface at the sample's center (Fig. 2). Stresses relax by the nucleation and propagation of dislocations in M and the reorientation of the interface (Fig. 2). The interface pushes dislocations into the M region and they almost do not penetrate into A. At $t = 1.1$, both M and A nucleate at the upper right and left corners, respectively. While the A region grows, its interface is getting almost parallel to the slip direction and up to three dislocations are inherited and arrested in A at the upper left corner. In the middle of a sample, the M embryo ($\eta \simeq 0.2$) appears, in which the dislocations nucleate, since $L_\xi > 0$ in the embryo. After parametric study and course graining, these results can lead to the constitutive equations for inheritance of the plastic strain and dislocation density for sharp interface models.[17]

Growth and arrest of a martensitic plate: A rectangular sample of the size of 67×20 is considered. As an initial condition, a martensitic rectangular nucleus of the size of 5×3 is located at the lower left corner of the sample. Four dislocation systems inclined at $\pm 60°$ (Fig. 3) are included. Material parameters are: $\beta_\xi = 7.5 \times 10^{-11}$N, $A_\alpha = 0.75$ GPa for A, $A_\alpha = 2.25$ GPa for M, $\gamma = 0.5$, $A_0 = 6$ MPa K^{-1}, $\varepsilon_t^y = 0.137$, $\varepsilon_t^x = \gamma_{yx} = 0$, and $\gamma_{xy} = 0.259$.

Without dislocations, the martensitic nucleus disappears at $\tilde{\theta} < 0.39$. For $\tilde{\theta} \geq 0.39$, the M propagates through the entire length of the sample and creates a martensitic plate of the equilibrium width, which increases with increasing $\tilde{\theta}$

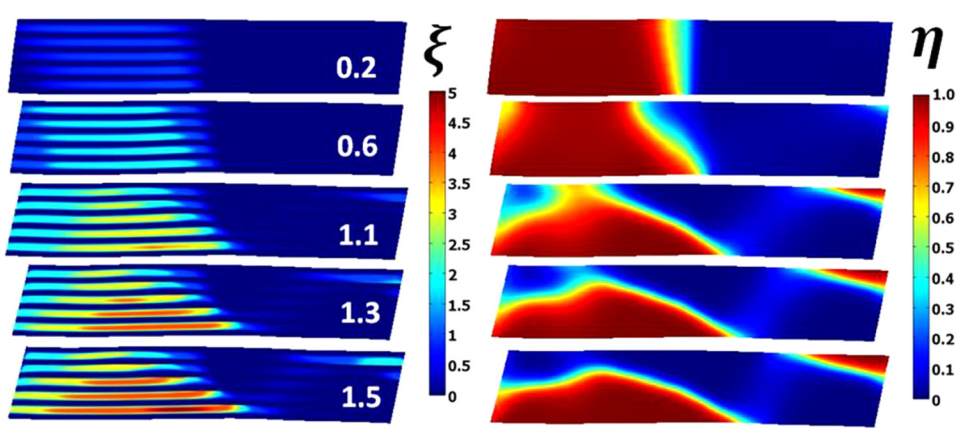

FIG. 2. Coupled evolution of phase (right) and dislocation (left) systems in a central 30×5.6 part of a rectangular 36×15 sample under simple shear for $\tilde{\theta} = 1.17$.

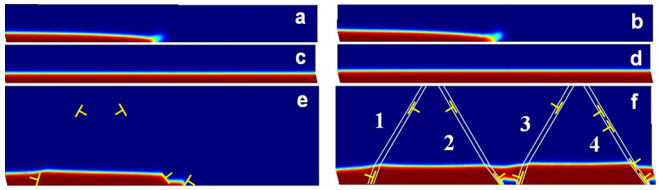

FIG. 3. Martensitic plate in the intermediate ((a) and (b)) and stationary ((c) and (d)) states for $\tilde{\theta} = 0.39$ (left) and $\tilde{\theta} = 0.49$ (right) for the case without plasticity in a part of a rectangular sample of the size of 67×20. For the case with dislocations, the stationary solutions are shown in the entire sample with four slip planes, in the same scale as in (a)-(d), for $\tilde{\theta} = 0.39$ (e) and $\tilde{\theta} = 0.49$ (f).

(Fig. 3(a)). For the coupled problem, dislocations nucleate at the tip of the plate and propagate within the sample. At some stage, dislocation of the opposite sign nucleates and remains within the M plate for slip plane 1 and 2. For $\tilde{\theta} = 0.39$, the M plate is arrested by two dislocations in the middle of a sample. In the region of compressive stresses near dislocations, significant thinning of the plate is observed. This nanostructure remains stable up to $\tilde{\theta} = 0.49$, after which growth continues until the right end of the sample with observable thickening. In the slip plane 3, dislocation appears near the M tip, then, with propagation of M plate, it disappears and then dislocations of the opposite sign appear one after another. Since nucleation near the free surface is easier, two pairs of two dislocations of the opposite sign appear. Some of dislocations are inherited by M. Two regions of residual A remain in the regions of compressive stresses near dislocations. Thus, the generation of dislocations produces athermal friction and arrests the plate at small driving force. For the case in study, athermal friction is $\Delta\tilde{\theta} = 0.1$ (corresponding to undercooling of $\Delta\theta = 40\,\mathrm{K}$ or energy barrier of 80 MPa), which is smaller than for dislocations within interface in Fig. 1. When athermal friction can be overcome at lower temperature, the width of the M plate is larger than in the case without dislocations due to stress relaxation. The obtained results explain the arrest of M by plastic accommodation and possible morphological transition from plate to lath martensite. This transition is technologically important and may be used to control nanostructure and properties by controlling the yield strength,[5,6,15] e.g., by alloying.

To summarize, a PFA to coupled martensitic PT and dislocation evolution is developed and a number of model problems for temperature and stress-induced PTs interacting with dislocation evolution are solved. Various experimental phenomena are reproduced and some effects are revealed. These results can be used for the development of the larger-scale models. A similar approach can be developed for the interaction of complete and partial dislocations with twins and diffusive PTs, as well as electromagnetic and reconstructive PTs. Dislocation reactions, especially of inherited dislocations, can be included as well.

The support of NSF, ARO, DARPA, and ISU is gratefully acknowledged.

[1]F. D. Fischer, G. Reisner, E. Werner, K. Tanaka, G. Cailletaud, and T. Antretter, Int. J. Plast. **16**, 723 (2000).
[2]F. Delogu, Acta Mater. **59**, 2069 (2011).
[3]C. Ji, V. I. Levitas, H. Zhu, J. Chaudhuri, A. Marathe, and Y. Ma, Proc. Natl. Acad. Sci. U.S.A. **109**, 19108 (2012); V. I. Levitas, Y. Z. Ma, and J. Hashemi, Appl. Phys. Lett. **86**, 071912 (2005).
[4]V. I. Levitas, Phys. Rev. B **70**, 184118 (2004).
[5]G. B. Olson and M. Cohen, *Dislocations in Solids*, edited by F. R. N. Nabarro (Elsevier, 1986), Vol. 7, pp. 297–407; G. B. Olson and A. L. Roitburd, *Martensite*, edited by G. B. Olson and W. S. Owen (ASM Interational, 1992), Chap. 9, pp. 149–174.
[6]G. B. Olson, Science **277**, 1237 (1997).
[7]Y. M. Jin, A. Artemev, and A. G. Khachaturyan, Acta Mater. **49**, 2309 (2001); L. Q. Chen, Annu. Rev. Mater. Res. **32**, 113 (2002); C. H. Lei, L. J. Li, Y. C. Shu, and J. Y. Li. Appl. Phys. Lett. **96**, 141910 (2010); A. V. Idesman, J. Y. Cho, and V. I. Levitas, *ibid*. **93**, 043102 (2008).
[8]V. I. Levitas and M. Javanbakht, Phys. Rev. Lett. **105**, 165701 (2010).
[9]V. I. Levitas, V. A. Levin, K. M. Zingerman, and E. I. Freiman, Phys. Rev. Lett. **103**, 025702 (2009).
[10]Y. U. Wang, Y. M. Jin, A. M. Cuitino, and A. G. Khachaturyan, Appl. Phys. Lett. **78**, 2324–2326 (2001); S. Y. Hu, Y. L. Li, Y. X. Zheng, and L. Q. Chen, Int. J. Plast. **20**, 403 (2004); S. Y. Hu, M. I. Baskes, and M. Stan, Appl. Phys. Lett. **90**, 081921 (2007).
[11]V. I. Levitas and M. Javanbakht, Phys. Rev. B **86**, 140101(R) (2012).
[12]A. L. Korzhenevskii, R. Bausch, and R. Schmitz, Phys. Rev. Lett. **91**, 236101 (2003); A. A. Boulbitch and P. Toledano, *ibid*. **81**, 838 (1998).
[13]A. C. E. Reid, G. B. Olson, and B. Moran, Phase Transitions **69**, 309 (1999); W. Zhang, Y. M. Jin, and A. G. Khachaturyan, Acta Mater. **55**, 565 (2007).
[14]J. Kundin, H. Emmerich, and J. Zimmer, Philos. Mag. **91**, 97 (2011).
[15]V. I. Levitas, A. V. Idesman, G. B. Olson, and E. Stein, Philos. Mag. A **82**, 429 (2002).
[16]See supplementary material at http://dx.doi.org/10.1063/1.4812488 for two figures which represent schematics for Burgers vectors and normals to the slip planes in austenite and martensite in different congurations and their transformations during phase transformations.
[17]V. I. Levitas, A. V. Idesman, and E. Stein, Int. J. Solids Struct. **35**, 855 (1998); A. V. Idesman, V. I. Levitas, and E. Stein, Int. J. Plast. **16**, 893 (2000).

Phase field approach to interaction of phase transformation and dislocation evolution

Valery I. Levitas[1] and Mahdi Javanbakht[2]

[1]*Iowa State University, Departments of Aerospace Engineering, Mechanical Engineering, and Material Science and Engineering, Ames, Iowa 50011, USA*

[2]*Iowa State University, Department of Mechanical Engineering, Ames, Iowa 50011, USA*

Supplementary Figures

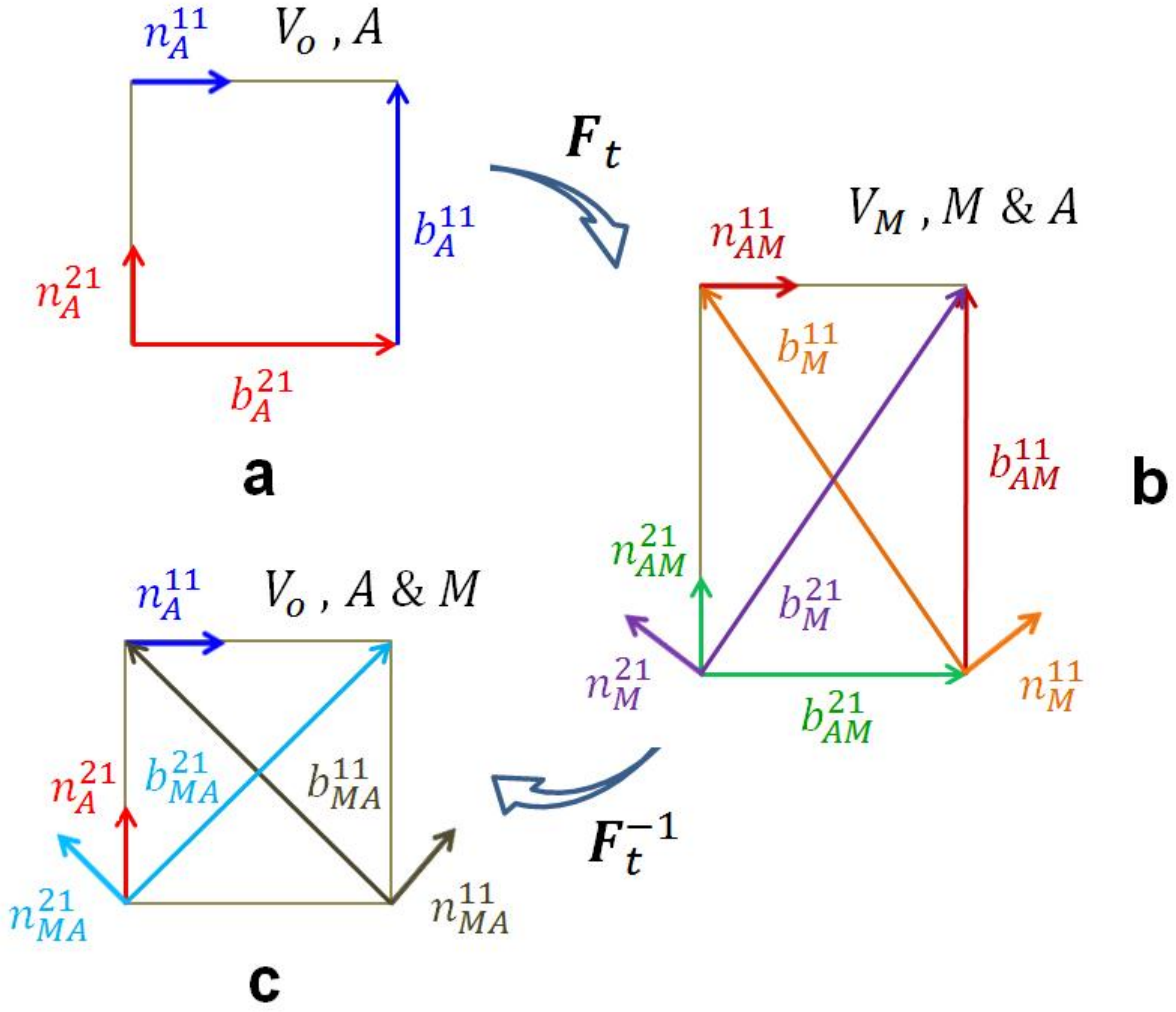

Figure 1: (color online). Schematics for Burgers vectors and normals to slip planes in austenite and martensite in different configurations and their transformations during phase transformations. (a) Two dimensional fcc lattice of austenite with two slip systems ($\boldsymbol{b}_A^{\alpha\omega}$, $\boldsymbol{n}_A^{\alpha\omega}$) along the faces in the initial configuration V_0. (b) Two dimensional bcc lattice of martensite with two slip systems ($\boldsymbol{b}_M^{\alpha\omega}$, $\boldsymbol{n}_M^{\alpha\omega}$) along the diagonals in the transformed configuration V_M obtained from V_0 after applying transformation deformation gradient $\boldsymbol{F}_t$. Slip systems of austenite inherited by martensite ($\boldsymbol{b}_{AM}^{\alpha\omega} = \boldsymbol{F}_t \cdot \boldsymbol{b}_A^{\alpha\omega}$, $\boldsymbol{n}_{AM}^{\alpha\omega} = \boldsymbol{n}_A^{\alpha\omega} \cdot \boldsymbol{F}_t^{-1}/|\boldsymbol{n}_M^{\alpha\omega} \cdot \boldsymbol{F}_t^{-1}|$) are shown as well. (c) Slip systems of martensite inherited by austenite ($\boldsymbol{b}_{MA}^{\alpha\omega} = \boldsymbol{F}_t^{-1} \cdot \boldsymbol{b}_M^{\alpha\omega}$, $\boldsymbol{n}_{MA}^{\alpha\omega} = \boldsymbol{n}_M^{\alpha\omega} \cdot \boldsymbol{F}_t/|\boldsymbol{n}_M^{\alpha\omega} \cdot \boldsymbol{F}_t|$) during reverse phase transformation are shown in the reference configuration. Even if material is in the martensitic state, since all calculations are performed in the undeformed state, all slip systems in the configuration V_M should be pulled back to V_0 with the reverse transformation deformation gradient $\boldsymbol{F}_t^{-1}$. Since under such operations slip systems of martensite ($\boldsymbol{b}_M^{\alpha\omega}$, $\boldsymbol{n}_M^{\alpha\omega}$) transform to ($\boldsymbol{b}_{MA}^{\alpha\omega}$, $\boldsymbol{n}_{MA}^{\alpha\omega}$) and slip system of austenite in martensite ($\boldsymbol{b}_{AM}^{\alpha\omega}$, $\boldsymbol{n}_{AM}^{\alpha\omega}$) transform to slip system of austenite in austenite ($\boldsymbol{b}_A^{\alpha\omega}$, $\boldsymbol{n}_A^{\alpha\omega}$), Fig. S1 c contains all slip systems necessary for solution of the problem, namely ($\boldsymbol{b}_A^{\alpha\omega}$, $\boldsymbol{n}_A^{\alpha\omega}$) and ($\boldsymbol{b}_{MA}^{\alpha\omega}$, $\boldsymbol{n}_{MA}^{\alpha\omega}$).

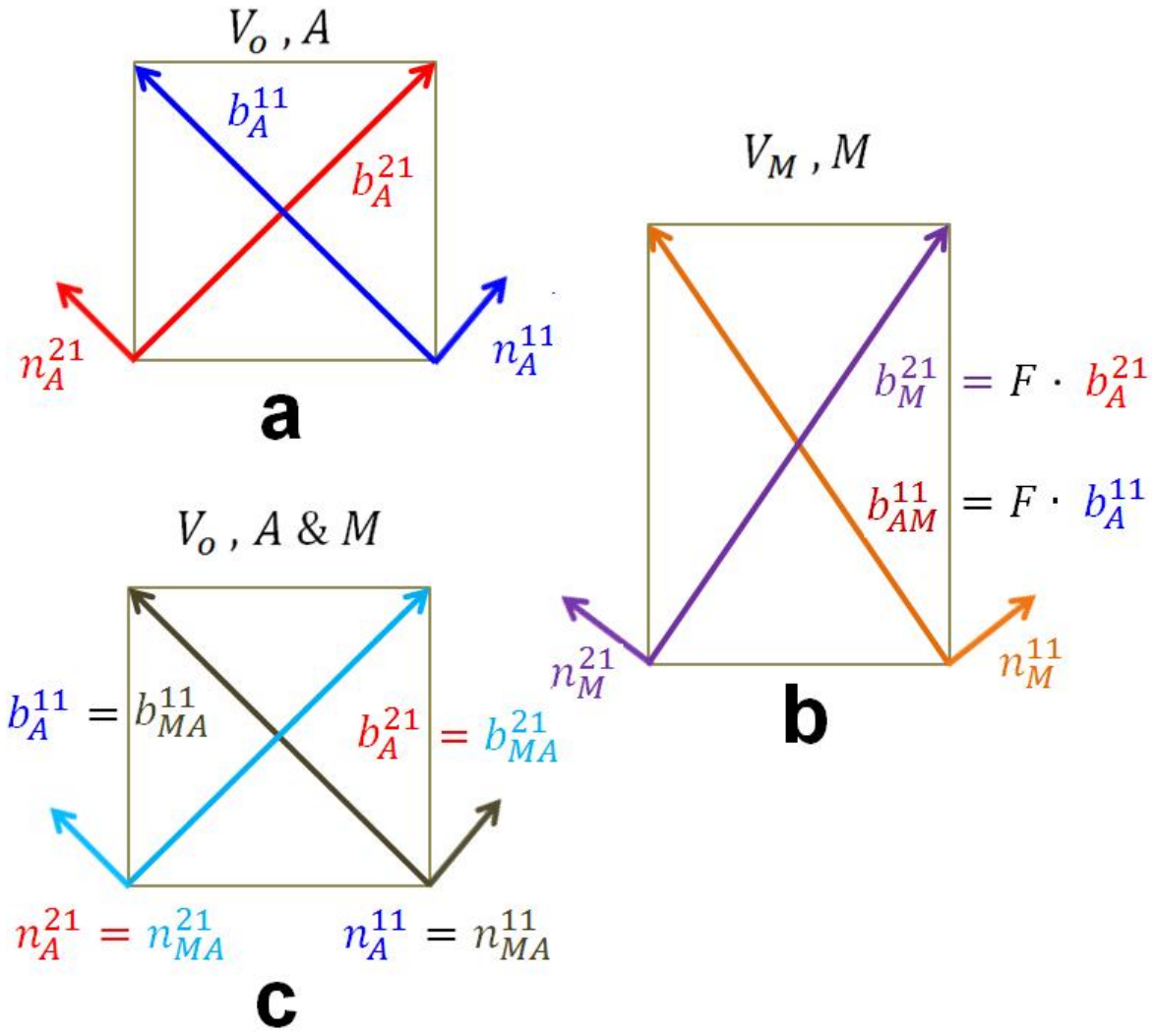

Figure 2: (color online). Schematics for Burgers vectors and normals to slip planes in austenite and martensite in the deformed V_0 and transformed V_M configurations and their transformations during phase transformations for the case when slip system of martensite ($\boldsymbol{b}_M^{\alpha\omega}$, $\boldsymbol{n}_M^{\alpha\omega}$) coincide with the transformed slip systems austenite ($\boldsymbol{b}_{AM}^{\alpha\omega} = \boldsymbol{F}_t \cdot \boldsymbol{b}_A^{\alpha\omega}$, $\boldsymbol{n}_{AM}^{\alpha\omega} = \boldsymbol{n}_A^{\alpha\omega} \cdot \boldsymbol{F}_t^{-1}/|\boldsymbol{n}_M^{\alpha\omega} \cdot \boldsymbol{F}_t^{-1}|$), i.e., $\boldsymbol{b}_M^{\alpha\omega} = \boldsymbol{F}_t \cdot \boldsymbol{b}_A^{\alpha\omega}$ and $\boldsymbol{n}_M^{\alpha\omega} = \boldsymbol{n}_A^{\alpha\omega} \cdot \boldsymbol{F}_t^{-1}/|\boldsymbol{n}_M^{\alpha\omega} \cdot \boldsymbol{F}_t^{-1}|$. (a) Two dimensional bcc lattice of austenite with two slip systems ($\boldsymbol{b}_A^{\alpha\omega}$, $\boldsymbol{n}_A^{\alpha\omega}$) along the diagonals in the initial configuration V_0. (b) Two dimensional bct lattice of martensite with two slip systems ($\boldsymbol{b}_M^{\alpha\omega}$, $\boldsymbol{n}_M^{\alpha\omega}$) along the diagonals in the transformed configuration V_M, which coincide with slip systems of austenite inherited by martensite ($\boldsymbol{b}_{AM}^{\alpha\omega}$, $\boldsymbol{n}_{AM}^{\alpha\omega}$). (c) Slip systems of martensite inherited by austenite ($\boldsymbol{b}_{MA}^{\alpha\omega}$, $\boldsymbol{n}_{MA}^{\alpha\omega}$) during reverse phase transformation in the reference configuration V_0. They coincide with the slip systems of austenite in austenite in V_0, i.e., ($\boldsymbol{b}_A^{\alpha\omega}$, $\boldsymbol{n}_A^{\alpha\omega}$). Thus, the only slip systems necessary for solution of the problem are slip systems of austenite in austenite in V_0, i.e., ($\boldsymbol{b}_A^{\alpha\omega}$, $\boldsymbol{n}_A^{\alpha\omega}$).